Reversible Optical Control of Conjugated Polymer Solubility with Sub-micrometer Resolution

Ian E. Jacobs,[†] Jun Li,[†] Stephanie L. Burg,[†] David J. Bilsky,[†] Brandon T. Rotondo,[†] Matthew P. Augustine,[‡] Pieter Stroeve,[†] and Adam J. Moulé*,[†]

[†]Department of Chemical Engineering and Materials Science and [‡]Department of Chemistry, University of California, Davis, California, United States

ABSTRACT Organic electronics promise to provide flexible, large-area circuitry such as photovoltaics, displays, and light emitting diodes that can be fabricated inexpensively from solutions. A major obstacle to this vision is that most conjugated organic materials are miscible, making solution-based fabrication of multilayer or micro- to nanoscale patterned films problematic. Here we demonstrate that the solubility of prototypical conductive polymer poly(3-hexylthiophene) (P3HT) can be reversibly "switched off" using high electron affinity molecular dopants, then later recovered with light or a suitable dedoping solution. Using this technique, we are able to stack mutually soluble materials and laterally pattern polymer films by evaporation or with light, achieving sub-micrometer, optically limited feature sizes. After forming these structures, the films can be dedoped without disrupting the patterned features; dedoped films have identical optical characteristics, charge carrier mobilities, and NMR spectra as as-cast P3HT films. This method greatly simplifies solution-based device fabrication, is easily adaptable to current manufacturing workflows, and is potentially generalizable to other classes of materials.

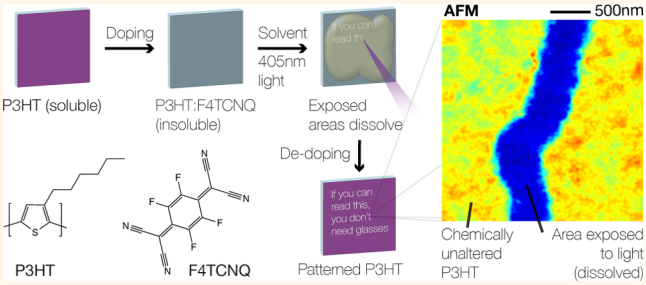

KEYWORDS: conductive polymers · doping · patterning · photolithography · solubility

Two major factors have driven research interest in organic electronics in recent years: the ability to easily tune material properties chemically and the potential to manufacture inexpensive, large-area devices by solution processing. Products taking advantage of chemical tunability, allowing for fine adjustment of material properties such as fluorescence or phosphorescence in small-molecule organic light-emitting diode (OLED) displays, have already entered the marketplace. However, despite intense research interest in applying low-cost, large-area printing techniques such as inkjet printing to organic semiconductors,[1−5] almost all commercial organic electronics are manufactured by comparatively costly vacuum deposition techniques, limiting material choices to small molecules or oligomers.

The major roadblock to solution-processed organic devices is the high mutual solubility of conjugated organic materials (COMs). Promising applications such as displays or sensor arrays require complex, 3-D arrangements of different materials on a single substrate, which necessitates methods to limit mixing or spatially separate deposited solutions. For example, in small-molecule photovoltaics and OLEDs, devices composed of five or more stacked organic layers are not uncommon.[6−10] Organic architectures that are this complex are currently only possible using evaporative deposition of small molecules. Similar issues are often encountered in biomedical and optical materials.[11] Solution processing is potentially cheaper for large-area deposition and allows for the use of polymers as well as small molecules. But patterning of solution-processed materials requires a combination of methods to reduce miscibility of stacked materials and/or spatially separate miscible materials. Bilayer deposition is possible in specific cases where orthogonal solvents for two materials can be found,[12,13] but for applications where several different stacked materials are required, this approach fails, as

* Address correspondence to amoule@ucdavis.edu.

Received for review November 30, 2014 and accepted January 14, 2015.

Published online January 14, 2015
10.1021/nn506820d

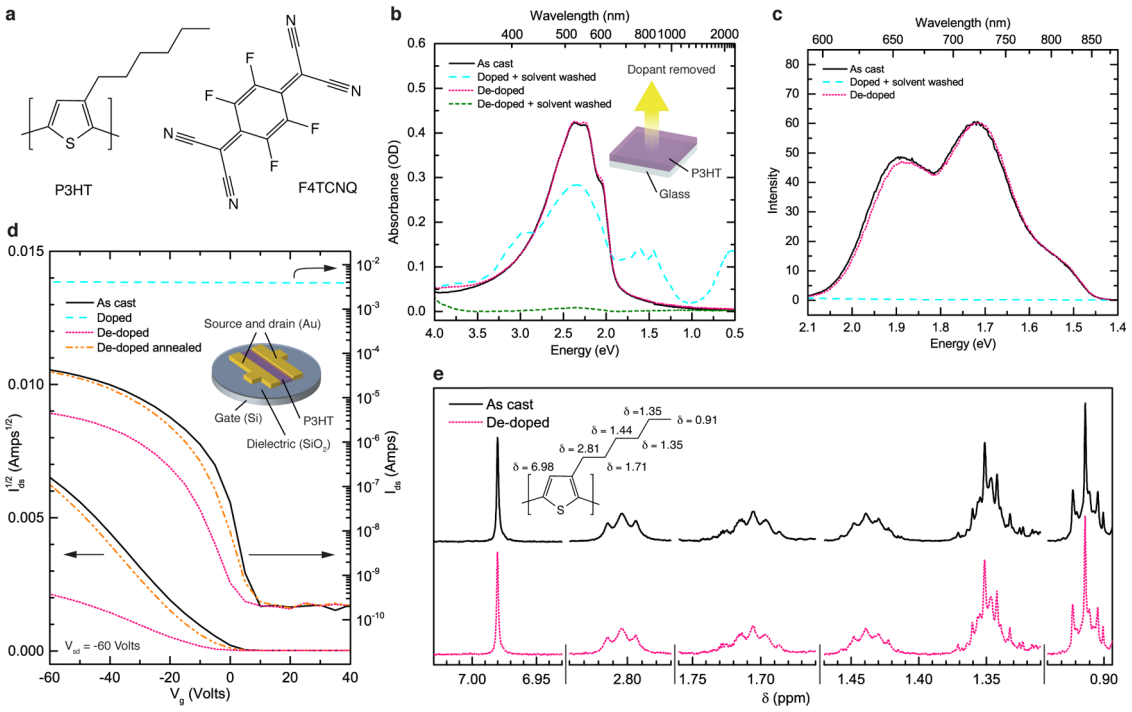

Figure 1. Demonstration of reversible doping induced solubility control in P3HT. (a) Structures of P3HT and F4TCNQ. (b) UV−vis−NIR absorption, (c) photoluminescence spectra, and (d) OFET transfer curves of a thin film of P3HT as-cast, after doping and rinsing with CB, after dedoping, and after rinsing with chloroform, showing complete recovery of as-cast optical properties and solubility. After annealing, transistor characteristics recover as well. (e) Details of ^{1}H NMR spectra of P3HT films as-cast and dedoped, redissolved in chloroform-D. Chemical shifts assignments for P3HT[36] are shown in the inset.

most COMs are soluble in a range of solvents. Even in the cases where orthogonal solvents can be found, specific tuning to individual material combinations and device architectures is necessary to minimize mixing. Spatial separation is achievable with printing techniques, but precise control of feature size, placement, and thicknesses requires prepatterned substrates,[2,3,14] due to surface energy effects, which affect most printing and coating techniques.[15] Even printing a single layer of unmodified COMs using standard inkjet printing gives rise to nonuniform pixels due to fluid dynamics. Clearly, building a 3-D, fully solution-processed device requires new approaches.

Proposed solutions to these deposition issues include cross-linking reactions,[16−19] tailored synthesis,[14,20] self-assembly,[21] orthogonal solvents,[12,13] evaporated protecting layers,[8] improved photoresists,[13,22−26] soft lithography,[21,27−29] and surface-directed patterning.[2,3,11,14,28] Unfortunately, none of these methods are universally effective and many require numerous processing steps, reducing the cost advantage of solution-processing. Cross-linking reactions permanently alter the chemical structure and generally require chemical tailoring, which usually results in degraded material properties.[16−19] Photoresists modified for compatibility with organics require either numerous complex processing steps or fluorinated solvents[2,3,13,22−25] and do not allow for multilayer devices, *e.g.*, stacking two mutually soluble polymers. Other techniques such as soft lithography are not easily applied to devices requiring pattering over disparate length scales[5,21,27,29,30] or requiring precise alignment. In short, despite the promise of cheap, solution-processed large-area electronics, the lack of a disruptive patterning methodology, like photolithography was for inorganic semiconductors, is holding back commercial adoption of polymeric electronics. Here, we present a candidate for such a process.

RESULTS AND DISCUSSION

Our technique, dopant-induced solubility control (DISC), is based on the observation that the solubility of semiconducting polymers can be reversibly controlled by doping with high electron affinity molecules. Figure 1a shows the structures of the prototypical semiconducting polymer regioregular poly(3-hexylthiophene) (P3HT) and molecular dopant 2,3,5,6-tetrafluoro-7,7,8,8-tetracyanoquinodimethane (F4TCNQ) When P3HT and F4TCNQ are mixed, charge is transferred from P3HT to F4TCNQ,[31−35] which renders the polymer insoluble in a wide range of solvents (Figure S1).

Reversible solubility control is demonstrated in a straightforward experiment: a thin film of P3HT is coated onto glass from a chlorobenzene (CB) solution, then doped by immersion in a dilute F4TCNQ/acetone solution to render the film insoluble, and finally rinsed with CB to verify that the film is insoluble. To reverse the process, the film is dedoped by immersion in a

solution of acetone and ethylenediamine. As seen in Figure 1b and c, upon dedoping we observe complete recovery of the $\pi-\pi^*$ absorption (1.9−2.2 eV) and photoluminescence (1.4−2.0 eV) bands of P3HT, both of which are quenched by doping interactions.[37] Complete fluorescence recovery implies that a vanishingly small F4TCNQ density remains in the film or that the remaining F4TCNQ has all reacted with ethylenediamine to form a nondoping product. Dedoped films show no change in thickness or solubility compared to as-cast films despite having been rinsed with CB while doped. Figure 1e shows ^{1}H NMR spectra of as-cast and dedoped films redissolved in chloroform-D, verifying that no chemical modification of the polymer occurs during this procedure. The dedoped + solvent washed curve in Figure 1b shows little residue left after redissolving the film in chloroform-D, indicating that the solution-state NMR spectra are representative of the entire film. In addition, AFM images (Figure S2) show minimal changes to film RMS roughness, increasing from 2.85 nm as cast to 3.07 nm after doping and 3.26 nm after dedoping.

To establish that the electrical properties of the polymer are similarly recoverable, we fabricate organic field effect transistors (OFETs) using P3HT as the active layer and subject them to the same doping and dedoping procedure used in the optical measurements. Although still quite functional, we do not observe complete recovery upon dedoping, which is attributed to irreversible morphological changes due to extended solvent exposure (~17 min total) during the procedure. Upon modifying the procedure to minimize solvent contact time (approximately 20 s total, using the same doping and dedoping solutions; see Methods section), we obtain the transfer curves shown in Figure 1d. After a short annealing step, the dedoped device returns almost exactly to as-cast device performance. These devices show on/off ratios of $>10^5$, with off currents limited by the sensitivity of our instrumentation. Saturation-regime mobilities[38] are unchanged at μ = 0.07 cm^2/V s for both as-cast and dedoped annealed devices, comparable to the state-of-the-art for P3HT of 0.1 cm^2/V s,[1,38] demonstrating that DISC processing does not adversely affect even high-performance devices. Figure S3 shows OFET transfer curves for devices fabricated using the immersion-based doping and dedoping procedure.

An illustrative application for DISC would be to stack mutually soluble materials, such as an OLED on top of an OTFT in an active-matrix display.[4,39] Poly[(9,9-di-*n*-octylfluorenyl-2,7-diyl)-*alt*-(benzo[2,1,3]thiadiazol-4,8-diyl)] (F8BT) is a yellow-green emitting polymer commonly used in OLEDs that is soluble in similar solvents to P3HT.[40] Figure 2a and b show UV−vis−NIR and photoluminescence spectra of an F8BT film spin-coated from CB on top of doped P3HT. The P3HT layer is then dedoped with the F8BT layer still in place,

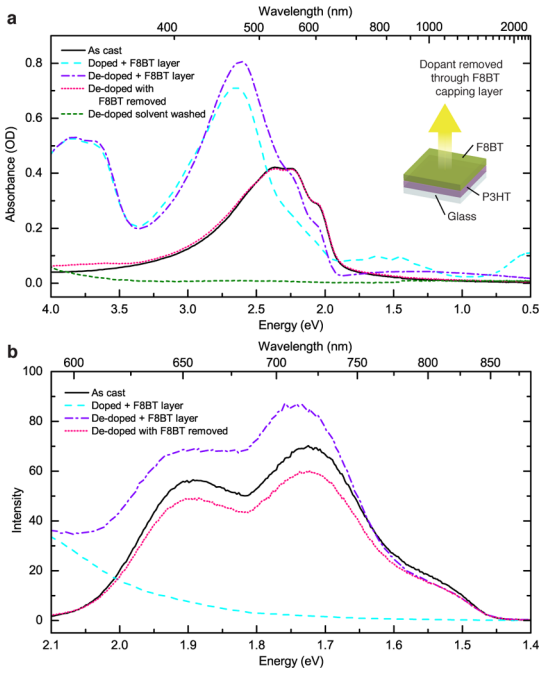

Figure 2. Fabrication of stacked mutually soluble polymers. (a) UV−vis−NIR absorption and (b) photoluminescence spectra of P3HT as-cast, doped then coated with F8BT, dedoped with F8BT layer still in place, after removal of the F8BT layer, and after rinsing with chloroform, demonstrating the ability to dedope through multilayer stacks.

verified by the recovery of vibronic features in the absorption spectrum at 2.0 and 2.25 eV and the recovery of photoluminescence. F8BT is known to quench P3HT excitons,[41] so recovery of photoluminescence after dedoping suggests that the film contains discrete P3HT and F8BT layers. Upon removal of the F8BT by an orthogonal solvent, we observe nearly complete recovery of as-cast absorption and photoluminescence.

Although the electron affinity of F4TCNQ is insufficient to dope most other conductive polymers,[31] the mechanism extends to other material combinations. Iodine has been studied as a neutral molecular dopant for COMs,[42] and we observe similar inhibition of solubility upon doping P3HT or MEH-PPV (poly[2-methoxy-5-(2-ethylhexyloxy)-1,4-phenylenevinylene]), a highly amorphous[43] conducting polymer, with iodine vapor (see Figure S4). Also, as seen in Figure S5, when F4TCNQ-doped films are immersed in "good" solvents for P3HT, crystalline domains swell with solvent but do not dissolve, even at low doping levels, where F4TCNQ resides in amorphous domains of P3HT.[32,35] These observations together suggest that the reduction in polymer solubility is not simply a result of cocrystallization of [polymer$^+$]:[dopant$^-$]. No new covalent bonds between the polymer and itself or dopants are expected to form or observed on the time scales of the doping and dedoping process; it therefore appears that reversible charge-transfer interactions[44] are central to the mechanism. In this case, the technique

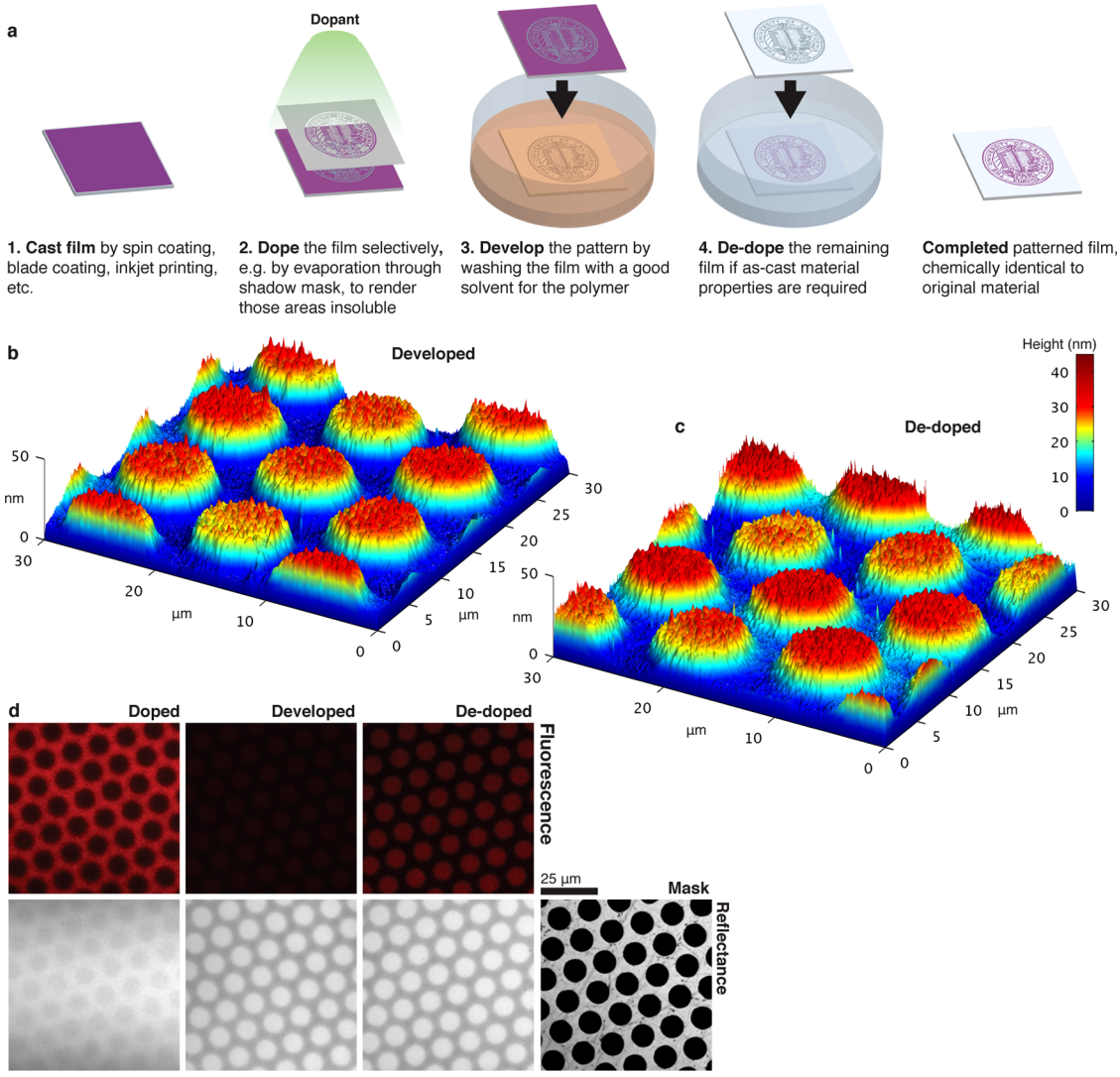

Figure 3. Additive patterning. (a) Schematic of the additive patterning process. (b and c) Atomic force (AFM) micrographs of P3HT films patterned by evaporation of F4TCNQ though a 2000 mesh TEM grid and developed with ODCB, after the developing step and after the dedoping step. (d) Laser scanning confocal micrographs showing reflectance (bottom) and photoluminescence (top) after doping, developing, and dedoping steps. Doped areas appear dark in the photoluminescence images, while undoped regions appear bright. Photoluminescence images are false-colored. A reflectance image of the mask is shown lower right, along with a 25 μm scale bar.

could be generalized to a wide variety of COMs if suitable dopant materials are designed.

ADDITIVE PATTERNING

By controlling doping (and thereby solubility) in specified areas of the film, we can use DISC to pattern P3HT at high resolution. Two solution-based patterning techniques are demonstrated below.

In the "additive process", we add dopants to an initially undoped film, then develop the pattern by disolving away the undoped areas. The dopant can be introduced by various printing or vacuum deposition techniques; here, the process is demonstrated by thermally evaporating F4TCNQ through a transmission electron microscopy (TEM) grid used as a shadow mask. Figure 3a shows a schematic of this method. After developing the pattern with *o*-dichlorobenzene (ODCB), atomic force microscopy (Figure 3b) reveals flat, well-defined features corresponding to the holes in the TEM grid. Dedoping (Figure 3c) does not significantly affect feature size. Film roughness is comparable to the doped and dedoped films in Figure S2, with RMS roughnesses of 2.33 nm after developing and 2.85 nm after dedoping. Areas between the patterned features are significantly smoother, with a roughnesses of 1.44 nm after developing and 1.85 nm after dedoping. In addition, the height of the patterned features matches the film thickness, as measured by profilimeter. This suggests an only very thin layer of material, if any, remains between the patterned areas.

The process is also visualized by laser scanning confocal microscopy, shown in Figure 3d; fluorescence images are shown above with corresponding reflectance images below. Doping quenches

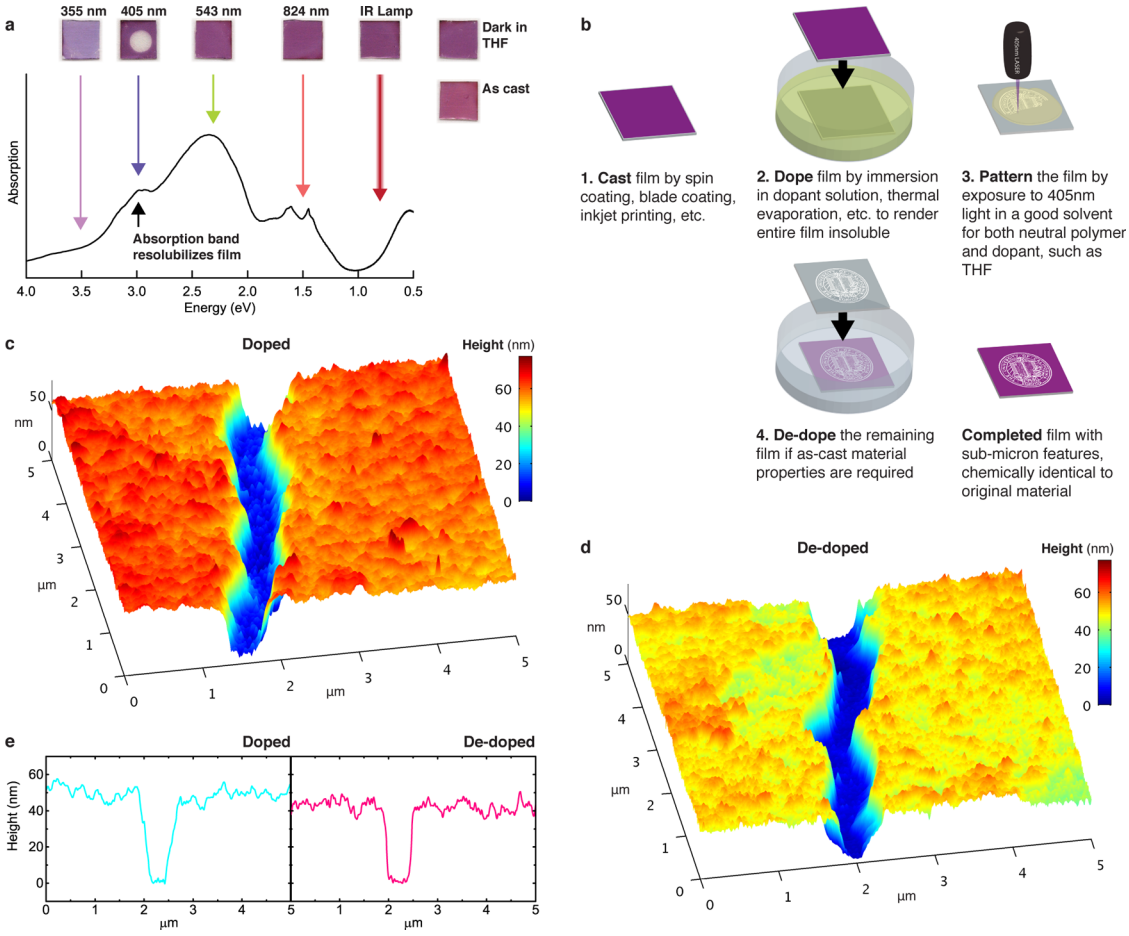

Figure 4. Subtractive patterning. (a) UV−vis−NIR spectra of P3HT:F4TCNQ and images of films immersed in THF and illuminated at indicated absorption bands at intensities of ~500 μW/cm^2 for 92 h. Note the dissolved circle in the slide illuminated at 3 eV (405 nm). See Figure S7 for UV−vis−NIR spectra of these films. (b) Schematic of the subtractive patterning technique. (c) AFM image showing a ~500 nm wide line drawn into a doped P3HT film immersed in THF using a 405 nm laser. (d) AFM image of the same line after dedoping. (e) Slices through the AFM images.

photoluminescence, so doped areas appear dark while undoped regions appear bright (false colored red). After evaporation, reflectance images show faint circular areas in the film corresponding to doped areas. This is confirmed by dark circles in the photoluminescence images. After developing, the undoped photoluminescent regions between the circles dissolve, seen by the increased contrast in the reflectance image and nearly black photoluminescence image. Dedoping does not affect the reflectance image, but is confirmed by recovery of photoluminescence. Low-magnification images (Figure S6) show that these features are uniformly reproduced over the full masked area (~ mm). These results suggest this process can reliably produce features as small as a few micrometers. We expect that resolution is primarily limited by the diffusion rate of the dopant and could be improved by engineering dopant molecules for reduced diffusion rates.

Although the additive DISC process requires the use of a separate patterning technique (*e.g.*, evaporation through a shadow mask or inkjet printing), it has inherent advantages. Since the film thickness is determined by the initial polymer thickness and films remain insoluble over a wide range of doping ratios, the resulting patterned features are inherently flat. This potentially allows for inkjet patterning of films while avoiding variations in thickness or morphology caused by mass transfer in droplets during solvent evaporation.[5,15] In addition, it enables evaporative patterning of polymer films otherwise only feasible for small molecules or atomic species.

SUBTRACTIVE PATTERNING

A second patterning method, the "subtractive process", begins with a uniformly doped film, from which dopants are selectively removed to render areas soluble. This is possible *via* an optical transition at 3 eV (~405 nm), labeled in the absorption spectrum of P3HT:F4TCNQ in Figure 4a. The inset shows P3HT:F4TCNQ films that were submerged in tetrahydrofuran (THF) and illuminated with low-intensity monochromatic light (~500 μW/cm^2 CW) for 92 h at the energies indicated by the arrows. Most of the films remain insoluble; however, the film illuminated at 3 eV dissolves

in the area exposed to light (visible by the transparent circle in the film). See Figure S7 for UV−vis−NIR spectra of these films. When exposed to light or solvent individually or sequentially, we observe no dissolution. At high light intensities, dissolution is near-instantaneous, permitting features to be written directly into the film. This effect cannot be simply attributed to local heating, since (1) at low light intensities no significant heating is expected, yet the film slowly dissolves when illuminated at 3 eV, and (2) under focused illumination dissolution is not observed at 2.28 eV (the strongest absorption band in the film) but is rapid at 3 eV.

This transition allows for a simple "direct-write" patterning method similar to photolithography, in which the polymer essentially acts as its own photoresist. A schematic of the technique is shown in Figure 4b. We demonstrate the method using a HD-DVD optical pickup (λ = 405 nm = 3.06 eV, beam waist ca. 500−600 nm) as the illumination source, due to its low cost (~$5), integrated low-aberration optics, and relatively long (~2 mm) working distance. Doped P3HT films were wetted with THF and scanned under the laser (exposure time on the order of ms) using a manually controlled micrometer stage. Figure 4c and d show atomic force micrographs of a line etched into a film of P3HT before and after dedoping, respectively. Line scans of these images are shown in Figure 4e. The process clearly achieves sub-micrometer resolution; additionally, dedoping does not affect feature sharpness. As the width of the patterned features matches the laser beam waist diameter (ca. 500−600 nm), we conclude that resolution is currently limited by the optical resolution of our experimental setup. Film roughness is not significantly affected by the patterning process, increasing from 2.79 nm RMS after patterning to 3.36 nm RMS after dedoping. These values are in line with what was observed for planar films (Figure S2). Within the patterned line, roughness decreases from 3.39 nm after patterning to 1.43 after dedoping, suggesting that some material remains after patterning but is removed after dedoping. This material is most likely the dopant. P3HT is moderately soluble in THF but completely insoluble in the dedoping solution; F4TCNQ on the other hand is only weakly soluble in THF, but dissolves rapidly in the dedoping solvent.

Figure S6 shows a photograph of the apparatus used, as well as a photograph of much larger (~100 μm) lines drawn into the film using a standard 5 mW 405 nm laser pointer. In addition, Figures S6 and S8 show optical and AFM micrographs of larger area films patterned at an optical power (11 mW/cm^2) and dose easily achievable using standard photolithography equipment. We clearly demonstrate sub-micrometer patterning control using low-cost optics and low-toxicity solvents in a bare-bones setup, suggesting that significant improvements are forthcoming.

CONCLUSION

In its ability to deposit or stack materials without allowing mixing, DISC is akin to a reversible cross-linking reaction. On the other hand, the ability to optically pattern films with sub-micrometer precision is compatible with direct-write immersion photolithography techniques, but requires fewer steps and no corrosive chemicals. Finally, the ability to pattern polymers by evaporation opens the door to introduction of polymeric materials in commercial OLED manufacturing workflows and suggests new research directions that may allow for better surface profile and morphological control in printing methods. Given the versatility of these techniques, we see a bright future for DISC in many areas of the emerging organic electronics industry and beyond, in fields such as optical and biomaterials processing.

METHODS

Reagents. P3HT (MW = 65 kDa, batches 11753 and 10560) was donated by Plextronics. F4TCNQ was purchased from TCI (98+%) and Sigma (97+%). F8BT (MW = 5−10 kDa) and MEH-PPV (MW = 150−250 kDa) were purchased from Sigma. All materials were used as received. Solvents were dried over 3A molecular sieves before use. Deuterated chloroform containing 0.03% TMS for NMR spectroscopy was sourced from Cambridge Isotope Laboratories.

Thin Film Preparation. Thin films were prepared by spin coating P3HT solutions (10 mg/mL in ODCB) at 60 °C onto clean, UV-ozone-treated 1 in. glass slides (Fisher Scientific). Film thicknesses were ~50 nm as measured by profilimeter (Veeco Dektak 150). For transistor measurements, silicon wafers (n-type ⟨100⟩, 300 nm oxide layer) were prepatterned with source and drain electrodes (1−2 nm Cr/80 nm Au) 50 μm length by 2 mm width. A trichlorododecylsilane self-assembled monolayer was prepared on the oxide layer before spin coating P3HT.

For bilayer samples, F8BT was spin-coated from CB (10 mg/mL) to form ~50 nm layers. The F8BT layers were removed with dichloromethane on the spin coater. MEH−-PPV films were prepared by spin coating from 10 mg/mL solutions in CB. Doped films in Figure S5 were spin coated from a mixed P3HT/F4TCNQ solution at 60 °C in chloroform, at a concentration of 1 mg/mL polymer basis.

All sample preparation, doping, and dedoping was performed inside a nitrogen glovebox equipped with a molecular sieve solvent trap.

Doping and Dedoping. P3HT films were doped by immersion into F4TCNQ solution (0.1 mg/mL in acetonitrile) at room temperature for 2 min. Dedoping was performed by soaking substrates in a 10:1 (v/v) acetone/ethylenediamine solution at 60 °C for 15 min, followed by washing with acetone on the spin coater. To verify recovery of solubility, films were redissolved in deuterated chloroform; these solutions were used for NMR spectroscopy. A modified method was developed for transistor measurements (Figure 1d). Doping was performed on the spin coater by coating the film with doping solution (as above), waiting 10 s, then spinning. Dedoping was accomplished by rinsing with 2 mL of dedoping solution (as above) at 60 °C while spinning. Annealing was performed at 150 °C for 10 min under nitrogen.

Iodine doping was performed by placing films into a jar containing solid iodine for 2 min, then rinsing with chloroform

to verify insolubility. Dedoping was performed by heating at 60 °C for 30 min under nitrogen.

Spectroscopy and Electrical Measurements. UV−vis−-NIR spectroscopy was performed on a PerkinElmer Lambda 750. Photoluminescence spectra were obtained on a Varian Cary Eclipse with λ_{ex} = 530 nm. Transistor measurements were performed using two Keithley 2420 sourcemeters connected to a home-built probe station in a nitrogen glovebox. Measurements were taken by sweeping the source voltage from positive to negative with respect to the drain at constant gate bias. NMR spectroscopy was performed in deuterated chloroform in 5 mm tubes on a 800 MHz Bruker Avance III spectrometer equipped with a cryoprobe. Chemical shifts were referenced to TMS.

Patterning and Microscopy. The sample in Figure 3 was prepared by thermally evaporating F4TCNQ through a transmission electron microscopy grid (2000 mesh, nickel, Ted Pella) taped to a P3HT film. Deposition was performed at 3×10^{-6} mbar, at a rate of ∼0.2 Å/s and total thickness of 2.5 nm as measured by a quartz microbalance. The film was developed in excess ODCB for ∼1 min.

The patterned P3HT films (Figures 4 and S8) were washed with THF on the spin coater after doping to remove any soluble material. The light source used in Figure S8 was a 405 nm handheld laser pointer, and in Figure 4 it was a PHR-803T HD-DVD optical pickup emitting at 405 nm. Optical power was ∼1.75 mW and ∼500 μW, respectively, as measured by a Newport 1918 power meter and 918D-UV-OD3R photodiode. Subtractive patterning in Figure S8 was performed by exposing the films for 5.5 min through a TEM grid (2000 mesh, nickel) in excess THF. Direct-write lithography was performed by wetting the film with THF and translating the slide in the focal plane of the laser; fine focus was attained by eye by maximizing the intensity of the solution-state P3HT fluorescence. The text in Figure S6 was patterned in a similar manner, except ODCB was used in place of THF and the light source was a 5 mW 405 nm laser pointer focused to a 50−100 μm spot size.

Atomic force microscopy (AFM) images were taken using a Veeco Multimode AFM in tapping mode. Laser scanning confocal microscopy was performed on an Olympus LSM-700 equipped with a 488 nm laser.

Photosolubility. Samples for Figures 4a and S8 were coated and doped as above, washed with THF, and placed into glass scintillation vials containing 5 mL of THF. Light sources used were a 355 nm UV lamp (approximately 250 μW/cm^2), a defocused 405 nm laser diode (∼800 μW/cm^2), a defocused 543 nm HeNe laser (∼1150 μW/cm^2), a 1000 W xenon arc lamp passed through a Newport Cornerstone 260 monochromator at 824 nm (∼450 μW/cm^2), and a 150 W infrared heat lamp (broadband, >1 mW/cm^2). The IR lamp sample was placed on a temperature-controlled cold plate set to 20 °C. Exposure time was 92 h.

Conflict of Interest: The authors declare no competing financial interest.

Acknowledgment. This research project was supported by the U.S. Department of Energy, Office of Basic Energy Sciences, Division of Materials Sciences and Engineering, under Award No. DE-SC0010419. The Bruker Avance 800 MHz NMR spectrometer was funded by NSF grant DBIO-722538. We also thank Plextronics Inc. for donation of P3HT, and W. D. Ristenpart for editing.

Supporting Information Available: Figures S1−S8 are available free of charge *via* the Internet at http://pubs.acs.org.

REFERENCES AND NOTES

1. Arias, A. C.; MacKenzie, J. D.; McCulloch, I.; Rivnay, J.; Salleo, A. Materials and Applications for Large Area Electronics: Solution-Based Approaches. *Chem. Rev.* **2010**, *110*, 3–24.
2. Sirringhaus, H.; Kawase, T.; Friend, R. H.; Shimoda, T.; Inbasekaran, M.; Wu, W.; Woo, E. P. High-Resolution Inkjet Printing of All-Polymer Transistor Circuits. *Science* **2000**, *290*, 2123–2126.
3. Minemawari, H.; Yamada, T.; Matsui, H.; Tsutsumi, J.; Haas, S.; Chiba, R.; Kumai, R.; Hasegawa, T. Inkjet Printing of Single-Crystal Films. *Nature* **2011**, *475*, 364–367.
4. Sirringhaus, H. 25th Anniversary Article: Organic Field-Effect Transistors: The Path beyond Amorphous Silicon. *Adv. Mater.* **2014**, *26*, 1319–1335.
5. de Gans, B.-J.; Duineveld, P.; Schubert, U. Inkjet Printing of Polymers: State of the Art and Future Developments. *Adv. Mater.* **2004**, *16*, 203–213.
6. Baldo, M. A.; Thompson, M. E.; Forrest, S. R. High-Efficiency Fluorescent Organic Light-Emitting Devices Using a Phosphorescent Sensitizer. *Nature* **2000**, *403*, 750–753.
7. Adamovich, V. I.; Cordero, S. R.; Djurovich, P. I.; Tamayo, A.; Thompson, M. E.; D'Andrade, B. W.; Forrest, S. R. New Charge-Carrier Blocking Materials for High Efficiency OLEDs. *Org. Electron.* **2003**, *4*, 77–87.
8. Lassiter, B. E.; Zimmerman, J. D.; Forrest, S. R. Tandem Organic Photovoltaics Incorporating Two Solution-Processed Small Molecule Donor Layers. *Appl. Phys. Lett.* **2013**, *103*, 123305.
9. Reineke, S.; Lindner, F.; Schwartz, G.; Seidler, N.; Walzer, K.; Lussem, B.; Leo, K. White Organic Light-Emitting Diodes with Fluorescent Tube Efficiency. *Nature* **2009**, *459*, 234–238.
10. Xue, J.; Uchida, S.; Rand, B. P.; Forrest, S. R. Asymmetric Tandem Organic Photovoltaic Cells with Hybrid Planar-Mixed Molecular Heterojunctions. *Appl. Phys. Lett.* **2004**, *85*, 5757–5759.
11. Nie, Z. H.; Kumacheva, E. Patterning Surfaces with Functional Polymers. *Nat. Mater.* **2008**, *7*, 277–290.
12. Rochester, C. W.; Mauger, S. A.; Moulé, A. J. Investigating the Morphology of Polymer/Fullerene Layers Coated Using Orthogonal Solvents. *J. Phys. Chem. C* **2012**, *116*, 7287–7292.
13. Zakhidov, A. A.; Lee, J.-K.; DeFranco, J. A.; Fong, H. H.; Taylor, P. G.; Chatzichristidi, M.; Ober, C. K.; Malliaras, G. G. Orthogonal Processing: A New Strategy for Organic Electronics. *Chem. Sci.* **2011**, *2*, 1178–1182.
14. Mei, J.; Diao, Y.; Appleton, A. L.; Fang, L.; Bao, Z. Integrated Materials Design of Organic Semiconductors for Field-Effect Transistors. *J. Am. Chem. Soc.* **2013**, *135*, 6724–6746.
15. Bonn, D.; Eggers, J.; Indekeu, J.; Meunier, J.; Rolley, E. Wetting and Spreading. *Rev. Mod. Phys.* **2009**, *81*, 739–805.
16. Muller, C. D.; Falcou, A.; Reckefuss, N.; Rojahn, M.; Wiederhirn, V.; Rudati, P.; Frohne, H.; Nuyken, O.; Becker, H.; Meerholz, K. Multi-Colour Organic Light-Emitting Displays by Solution Processing. *Nature* **2003**, *421*, 829–833.
17. Png, R.-Q.; Chia, P.-J.; Tang, J.-C.; Liu, B.; Sivaramakrishnan, S.; Zhou, M.; Khong, S.-H.; Chan, H. S. O.; Burroughes, J. H.; Chua, L.-L.; *et al.* High-Performance Polymer Semiconducting Heterostructure Devices by Nitrene-Mediated Photocrosslinking of Alkyl Side Chains. *Nat. Mater.* **2010**, *9*, 152–158.
18. Kim, B. J.; Miyamoto, Y.; Ma, B.; Fréchet, J. M. J. Photocrosslinkable Polythiophenes for Efficient, Thermally Stable, Organic Photovoltaics. *Adv. Funct. Mater.* **2009**, *19*, 2273–2281.
19. Tao, C.; Aljada, M.; Shaw, P. E.; Lee, K. H.; Cavaye, H.; Balfour, M. N.; Borthwick, R. J.; James, M.; Burn, P. L.; Gentle, I. R.; *et al.* Controlling Hierarchy in Solution-Processed Polymer Solar Cells Based on Crosslinked P3HT. *Adv. Energy Mater.* **2013**, *3*, 105–112.
20. Segalman, R. A.; McCulloch, B.; Kirmayer, S.; Urban, J. J. Block Copolymers for Organic Optoelectronics. *Macromolecules* **2009**, *42*, 9205–9216.
21. Menard, E.; Meitl, M. A.; Sun, Y. G.; Park, J. U.; Shir, D. J. L.; Nam, Y. S.; Jeon, S.; Rogers, J. A. Micro- and Nanopatterning Techniques for Organic Electronic and Optoelectronic Systems. *Chem. Rev.* **2007**, *107*, 1117–1160.
22. DeFranco, J. A.; Schmidt, B. S.; Lipson, M.; Malliaras, G. G. Photolithographic Patterning of Organic Electronic Materials. *Org. Electron.* **2006**, *7*, 22–28.
23. Hwang, H. S.; Zakhidov, A. A.; Lee, J.-K.; Andre, X.; DeFranco, J. A.; Fong, H. H.; Holmes, A. B.; Malliaras, G. G.; Ober, C. K. Dry Photolithographic Patterning Process for Organic Electronic Devices Using Supercritical Carbon Dioxide as a Solvent. *J. Mater. Chem.* **2008**, *18*, 3087–3090.

24. Dhar, B. M.; Kini, G. S.; Xia, G.; Jung, B. J.; Markovic, N.; Katz, H. E. Field-Effect Tuned Lateral Organic Diodes. *Proc. Natl. Acad. Sci. U.S.A.* **2010**, *107*, 3972–3976.
25. Shirota, Y. Photo- and Electroactive Amorphous Molecular Materials: Molecular Design, Syntheses, Reactions, Properties, and Applications. *J. Mater. Chem.* **2005**, *15*, 75–93.
26. Bahlke, M. E.; Mendoza, H. A.; Ashall, D. T.; Yin, A. S.; Baldo, M. A. Dry Lithography of Large-Area, Thin-Film Organic Semiconductors Using Frozen CO_2 Resists. *Adv. Mater.* **2012**, *24*, 6136–6140.
27. Xia, Y.; Whitesides, G. M. Soft Lithography. *Annu. Rev. Mater. Sci.* **1998**, *28*, 153–184.
28. Virkar, A. A.; Mannsfeld, S.; Bao, Z.; Stingelin, N. Organic Semiconductor Growth and Morphology Considerations for Organic Thin-Film Transistors. *Adv. Mater.* **2010**, *22*, 3857–3875.
29. Qin, D.; Xia, Y.; Whitesides, G. M. Soft Lithography for Micro- and Nanoscale Patterning. *Nat. Protocols* **2010**, *5*, 491–502.
30. Huang, Y. Y.; Zhou, W.; Hsia, K. J.; Menard, E.; Park, J.-U.; Rogers, J. A.; Alleyne, A. G. Stamp Collapse in Soft Lithography. *Langmuir* **2005**, *21*, 8058–8068.
31. Yim, K.-H.; Whiting, G. L.; Murphy, C. E.; Halls, J. J. M.; Burroughes, J. H.; Friend, R. H.; Kim, J.-S. Controlling Electrical Properties of Conjugated Polymers *via* a Solution-Based p-Type Doping. *Adv. Mater.* **2008**, *20*, 3319–3324.
32. Gao, J.; Roehling, J. D.; Li, Y.; Guo, H.; Moule, A. J.; Grey, J. K. The Effect of 2,3,5,6-Tetrafluoro-7,7,8,8-tetracyanoquinodimethane Charge Transfer Dopants on the Conformation and Aggregation of Poly(3-hexylthiophene). *J. Mater. Chem. C* **2013**, *1*, 5638–5646.
33. Pingel, P.; Neher, D. Comprehensive Picture of p-Type Doping of P3HT With the Molecular Acceptor F_4TCNQ. *Phys. Rev. B* **2013**, *87*, 115209.
34. Méndez, H.; Heimel, G.; Opitz, A.; Sauer, K.; Barkowski, P.; Oehzelt, M.; Soeda, J.; Okamoto, T.; Takeya, J.; Arlin, J.-B.; *et al*. Doping of Organic Semiconductors: Impact of Dopant Strength and Electronic Coupling. *Angew. Chem., Int. Ed.* **2013**, *52*, 7751–7755.
35. Duong, D. T.; Wang, C.; Antono, E.; Toney, M. F.; Salleo, A. The Chemical and Structural Origin of Efficient p-Type Doping in P3HT. *Org. Electron.* **2013**, *14*, 1330–1336.
36. Chen, T. A.; Rieke, R. D. The First Regioregular Head-to-Tail Poly(3-hexylthiophene-2,5-diyl) and a Regiorandom Isopolymer: Nickel *versus* Palladium Catalysis of 2(5)-Bromo-5(2)-(bromozincio)-3-hexylthiophene Polymerization. *J. Am. Chem. Soc.* **1992**, *114*, 10087–10088.
37. Brown, P. J.; Sirringhaus, H.; Harrison, M.; Shkunov, M.; Friend, R. H. Optical Spectroscopy of Field-Induced Charge in Self-Organized High Mobility Poly(3-hexylthiophene). *Phys. Rev. B* **2001**, *63*, 125204.
38. Dimitrakopoulos, C. D.; Malenfant, P. R. L. Organic Thin-Film Transistors for Large Area Electonics. *Adv. Mater.* **2002**, *14*, 99–117.
39. Sirringhaus, H.; Tessler, N.; Friend, R. H. Integrated Optoelectronic Devices Based on Conjugated Polymers. *Science* **1998**, *280*, 1741–1744.
40. Banach, M. J.; Friend, R. H.; Sirringhaus, H. Influence of the Casting Solvent on the Thermotropic Alignment of Thin Liquid Crystalline Polyfluorene Copolymer Films. *Macromolecules* **2004**, *37*, 6079–6085.
41. Facchetti, A. Polymer Donor-Polymer Acceptor (All-Polymer) Solar Cells. *Mater. Today* **2013**, *16*, 123–132.
42. Heeger, A. J.; Sariciftci, N. S.; Namdas, E. B. *Semiconducting and Metallic Polymers*; Oxford University Press, 2010.
43. Noriega, R.; Rivnay, J.; Vandewal, K.; Koch, F. P. V.; Stingelin, N.; Smith, P.; Toney, M. F.; Salleo, A. A General Relationship between Disorder, Aggregation and Charge Transport in Conjugated Polymers. *Nat. Mater.* **2013**, *12*, 1038–1044.
44. Bredas, J. L.; Norton, J. E.; Cornil, J.; Coropceanu, V. Molecular Understanding of Organic Solar Cells: The Challenges. *Acc. Chem. Res.* **2009**, *42*, 1691–1699.